ELSEVIER

Chemical Physics 182 (1994) 1–18

Chemical Physics

A perturbation theory treatment of oscillating magnetic fields in the radical pair mechanism

J.M. Canfield *[,a], R.L. Belford [b], P.G. Debrunner [a], K.J. Schulten [a,b,c]

[a] *Department of Physics, University of Illinois at Urbana-Champaign, Urbana, IL 61801, USA*
[b] *Department of Chemistry, University of Illinois at Urbana-Champaign, Urbana, IL 61801, USA*
[c] *Beckman Institute, University of Illinois at Urbana-Champaign, Urbana, IL 61801, USA*

Received 8 November 1993

Abstract

This paper describes an application of time-dependent perturbation theory to the calculation of singlet-to-triplet yields in radical pair reactions for oscillating magnetic fields. It outlines an iterative approach, based on the Schrödinger equation, that should hold for any order of perturbation theory and then gives explicit expressions up to second order in the oscillating field strength for the dependence of the singlet-to-triplet yield on the frequency of the oscillating field. It then compares this method to other methods, namely, numerical integration and the rotating frame treatment, and gives sample results for exponential and Noyes time-dependences. Finally, assuming the radical pair mechanism can explain certain magnetic field effects in biology, this paper discusses several counterintuitive behaviors of the singlet-to-triplet yields that may account for conflicts in the magnetic field bioeffects literature.

1. Introduction

This work was stimulated in part by the continued interest in the magnetic sense in animals [1,2] as well as the growing concern over health effects of subthermal electromagnetic fields [3,4]. One physical mechanism that has been proposed to account for biological effects of steady magnetic fields is the radical pair mechanism [5–9]. This mechanism has proven quite successful in explaining the effects of steady as well as microwave magnetic fields on the photosynthetic reaction center (see, for example, refs. [10–13]).

The purpose of this paper is to further examine the effects of oscillating magnetic fields on chemical reaction yields within the radical pair mechanism. It seeks a general treatment that can apply to a combination of a steady field with multiple oscillating fields, all at different frequencies and orientations with respect to the steady field. Since this work is aimed toward biological effects of magnetic fields and, in particular, magnetic sensory mechanisms, it should be sufficient to develop a general treatment that can hold in the natural magnetic environment. This is because the natural magnetic field undergoes slight variations in magnitude and direction with time and location, and these variations can provide information on direction, location, time of day, or season to animals capable of detecting them [14]. Thus, certain animals may have evolved sensitivity to the natural magnetic environment, and

* Corresponding author. Email: canfield@rlb6000.scs.uiuc.edu

SSDI 0301-0104 (93)E0442-X

effects due to man-made magnetic environments, which have not existed long on an evolutionary time-scale, are probably only incidental.

Thus, since the geomagnetic field is typically composed of a steady field of 0.5 G and a spectrum of oscillating fields with intensities well below 0.03 G (a fluctuation due to a very large magnetic storm) [14], in order to hold in the natural magnetic environment, the general treatment is restricted in that it must be able to handle very weak steady fields but enjoys the freedom that it can use perturbation theory to treat the effects of the oscillating fields. This use of perturbation theory should also be applicable to a number of man-made magnetic environments where the steady field is much larger than the oscillating fields. Thus, a general treatment based on perturbation theory should be useful in certain health effects studies as well.

2. Radical pair mechanism

2.1. Spin dynamics

The radical pair mechanism [15–17] holds when two unpaired electron spins ($\boldsymbol{S}_1$ and $\boldsymbol{S}_2$) coexist in a cage long enough to undergo spin dynamics (variation in singlet/triplet character with time) due, for example, to their interactions with external magnetic fields $\boldsymbol{B}(t)$ through the Zeeman effect, with nearby nuclear spins $\boldsymbol{I}_j$ through the hyperfine coupling a_j, and with each other via the exchange interaction J. Typically such a pair is formed in a singlet state by a homolytic cleavage of a covalent bond, and one needs to determine the chance that such a pair will escape rather than recombine. Since recombination typically occurs only in the singlet state [15], the spin dynamics and all the terms controlling it (such as the external magnetic field) are very important for determining the chance that the pair will escape. To quantify this chance for escape, one calculates the singlet-to-triplet yield Φ_{ST}.

To determine the singlet-to-triplet yield, one starts with an initial wavefunction $\psi(0)$ which is in a singlet state. Note that there are $N_S = \prod_j (2I_j + 1)$ such states, I_j being the nuclear spin of nucleus j, and one must average over the N_S different yields they give to obtain the overall singlet-to-triplet yield (this procedure is discussed in depth in ref. [18]).

Using each of these N_S different initial singlet wavefunctions $\psi(0)$, one then obtains N_S different wavefunctions at later times t by applying the Schrödinger equation:

$$\dot{\psi}(t) = \frac{\mathrm{d}\psi(t)}{\mathrm{d}t} = -\frac{\mathrm{i}}{\hbar} H(t)\psi(t) , \tag{1}$$

where the Hamiltonian $H(t)$ is typically a sum of Zeeman, hyperfine, and exchange interaction terms (all often assumed isotropic, as in the case of rapid tumbling in solution):

$$H(t) = g\mu_B \sum_{j=1}^{2} [\boldsymbol{B}(t)\cdot\boldsymbol{S}_j + a_j \boldsymbol{I}_j \cdot \boldsymbol{S}_j] + hJ\boldsymbol{S}_1 \cdot \boldsymbol{S}_2 . \tag{2}$$

Note that this Hamiltonian can in practice be much more complicated; for example, each interaction in it can be anisotropic (this requires replacement of the scalars g and a_j by matrices), there can be more than two nuclei having significant hyperfine interactions with the electron spins, and there can be terms for other interactions such as zero-field splitting and the electron dipole–dipole interaction. Nevertheless, Hamiltonian (2) is sufficient for the treatment given here.

Using the N_S different wavefunctions $\psi(t)$ obtained above, one can find N_S different triplet probabilities at time t:

$$P_{ST}(t) = \psi^*(t) Q_T \psi(t) , \tag{3}$$

where Q_T is the triplet projection operator:

$$Q_T = \tfrac{3}{4} + S_1 \cdot S_2 . \tag{4}$$

Note that for time-independent Hamiltonians each of these triplet probabilities $P_{ST}(t)$ varies in time like a sum of sines and cosines plus a constant term.

2.2. Cage dynamics

A pair of radicals is said to be in a cage as long as the radicals are near enough to interact only with each other, and the radicals are said to escape when they have diffused so far apart that they can no longer recombine. Thus, since the radical pair remains in the cage for a finite time and the overall recombination rate depends on how much triplet has formed during this lifetime, one calculates the N_S different singlet-to-triplet yields Φ_{ST} using

$$\Phi_{ST} = \int_0^\infty P_{ST}(t) f(t)\, dt , \tag{5}$$

where $f(t)$ is a function describing how many pairs remain at time t that can still undergo spin dynamics and have a chance to recombine. The function $f(t)$ is determined by the diffusion of the radicals in the pair. These radicals diffuse back and forth in the solvent, at times being separated by solvent molecules and at other times coming close enough to each other to have an encounter. At each encounter, radical pairs in the singlet state have a chance to recombine.

If the radical pair escapes from the cage after a single encounter, $f(t)$ can be given as an exponential decay [15,19]:

$$f(t) = \frac{1}{\tau} e^{-t/\tau}, \tag{6}$$

where τ is a constant as defined in ref. [15]. Nevertheless, if one needs to account for subsequent reencounter and recombination attempts, the Noyes weighting factor should be used instead [15,19]:

$$f(t) = Mt^{-3/2} e^{-A/t}, \tag{7}$$

where M and A are constants as defined in refs. [15,19]. Furthermore, if one needs to be even more rigorous, one can use an exact treatment of diffusion such as that given in ref. [20]. For simplicity, however, this paper will focus on the approximate exponential model.

Finally, having found the N_S different yields Φ_{ST}, one simply averages them all to obtain the overall singlet-to-triplet yield. Although the rest of this paper will not explicitly discuss these N_S different yields, one should realize that an average over these yields for each of the N_S different possible initial states must always be done.

3. Typical treatments of oscillating fields

3.1. Numerical integration

A most general way to determine $P_{ST}(t)$ and Φ_{ST} for time-dependent fields, $\boldsymbol{B}(t)$, is to integrate the Schrödinger equation (eq. (1)) using, for example, a fourth order Runge–Kutta scheme (a numerical method for solving ordinary differential equations [21]). This method can handle any time-dependent field, but, since it involves numerical integration, its accuracy depends on the time step δt and the number of steps N_t used. That is, if δt is too large, $P_{ST}(t)$ will deviate significantly from its true path, causing increasing inaccuracies as the number of time steps increases. Thus, this method usually requires a large number of very small time steps and, hence, tends to be

quite computationally intensive and slow. It also gives very little insight into how the singlet-to-triplet yield varies with magnetic field strength or frequency. Thus, a better method is desired.

3.2. Rotating frame treatment

If the magnetic field is of the form

$$\boldsymbol{B}(t) = B_0\hat{z} + B_1(\hat{x}\cos\omega t + \hat{y}\sin\omega t)\,, \tag{8}$$

where $\hat{x}$, $\hat{y}$, $\hat{z}$ are mutually perpendicular unit vectors in a right-handed basis, the resulting time-dependent Hamiltonian $H(t)$ can be transformed into a rotating frame where it becomes a time-independent Hamiltonian H'. One simply uses a unitary transformation matrix:

$$T(t) = \exp\left(\mathrm{i}\sum_{j=1}^{2}(S_{jz} + I_{jz})\,\omega t\right) \tag{9}$$

to convert the lab frame Hamiltonian $H(t)$ to the rotating frame Hamiltonian H'.

The transformation works as follows: since the rotating frame wave function $\psi'(t)$ is just $T(t)\psi(t)$ and $\psi(t) = T^{-1}(t)\psi'(t)$, in order for the Schrödinger equation to hold in both frames:

$$\dot{\psi}(t) = -\frac{\mathrm{i}}{\hbar}H(t)\psi(t) \tag{10}$$

and

$$\dot{\psi}'(t) = -\frac{\mathrm{i}}{\hbar}H'\psi'(t)\,, \tag{11}$$

one needs

$$H' = \mathrm{i}\hbar\dot{T}(t)T^{-1}(t) + T(t)H(t)T^{-1}(t)\,. \tag{12}$$

Thus, through eq. (2) and the relations given in ref. [22] for a general spin $\boldsymbol{I}$ with components I_x, I_y, and I_z:

$$U = \exp(\mathrm{i}\theta I_z)\,, \tag{13}$$

$$UI_xU^{-1} = I_x\cos\theta - I_y\sin\theta\,, \tag{14}$$

$$UI_yU^{-1} = I_y\cos\theta + I_x\sin\theta\,, \tag{15}$$

$$UI_zU^{-1} = I_z\,, \tag{16}$$

one obtains after some algebra

$$H' = g\mu_{\mathrm{B}}\sum_{j=1}^{2}(B_0S_{jz} + B_1S_{jx} + a_j\boldsymbol{I}_j\cdot\boldsymbol{S}_j) + hJ\boldsymbol{S}_1\cdot\boldsymbol{S}_2 - \hbar\omega\sum_{j=1}^{2}(S_{jz} + I_{jz})\,. \tag{17}$$

Note that the exponent of $T(t)$ includes the electron spin operators for the electrons that are involved in the Zeeman interaction with the rotating field $\boldsymbol{B}_1(t)$ as well as the nuclear spin operators for nuclei that couple to these electrons. If the Zeeman term due to the steady field $\boldsymbol{B}_0$ is large compared to the hyperfine and exchange terms (as in RYDMR experiments [11]), all the hyperfine terms change from $a_j\boldsymbol{I}_j\cdot\boldsymbol{S}_j$ to $a_jI_{jz}S_{jz}$. In this case the unitary transform

$$T(t) = \exp\left(\mathrm{i}\sum_{j=1}^{2}S_{jz}\,\omega t\right) \tag{18}$$

is sufficient, and the I_{jz} operators in the final term of H' can be neglected. In general, though, since a_j typically ranges from 0.5 to 100 G, for very weak steady fields, such as the earth's field of 0.5 G, it is important not to neglect these I_{jz} terms.

One important advantage of the rotating frame treatment is that it allows the time-dependent Hamiltonian $H(t)$ to be transformed into a time-independent Hamiltonian H', which allows quick and simple solution of its singlet-to-triplet yields. This method is also general in that the resultant Hamiltonian can be used in more complicated treatments such as those using the Liouville equation. This method is, however, limited to the case in which the only time-dependent field is rotating, the steady field is either negligible or along the axis of rotation of the rotating field, and the matrices of the Zeeman, hyperfine, and exchange terms are either isotropic or axially symmetric about the axis of the steady field. Thus, if one hopes to deal with more general field configurations, the interaction of multiple frequencies of oscillating field, or anisotropic Zeeman, hyperfine, or exchange interactions, this method will not suffice.

4. Perturbation theory treatment

4.1. General approach

4.1.1. Derivation

The first step in the perturbation theory treatment is to write the external magnetic field as

$$\boldsymbol{B}(t) = \boldsymbol{B}_0 + \boldsymbol{B}_1(t) \tag{19}$$

$$= \boldsymbol{B}_0 + \sum_{j=1}^{N_p} \boldsymbol{B}_{1j} \cos(\alpha_j t + \phi_j) \,, \tag{20}$$

where N_p is the number of oscillating fields applied. From this one obtains a time-dependent Hamiltonian $H(t)$ made up of a time-independent H_0 and a time-dependent perturbation $V(t)$:

$$H(t) = H_0 + V(t) \tag{21}$$

$$= H_0 + \sum_{j=1}^{N_p} V_j \cos(\alpha_j t + \phi_j) \,. \tag{22}$$

Then, as usual when applying perturbation theory, one must assume that $\boldsymbol{B}_1(t)$ and all its time-independent $\boldsymbol{B}_{1j}$ values are much smaller than B_0 in magnitude and that $V(t)$ and all its time-independent V_j matrices are much smaller than H_0 (or, equivalently, that the perturbations are applied for a very short time).

Next, as in ref. [23], one expresses the wavefunction as

$$\psi(t) = \sum_{n=1}^{N} b_n(t) \exp\left(-\frac{\mathrm{i}}{\hbar} E_n t\right) |n\rangle \,, \tag{23}$$

where $|n\rangle$ and E_n are eigenvectors and eigenvalues of the Hamiltonian H_0 satisfying $H_0|n\rangle = E_n|n\rangle$. Note that there are $N = 4N_S$ such eigenvectors and eigenvalues for the $N \times N$ matrix H_0.

Then, combining eqs. (1), (21), and (23) gives

$$\sum_{n=1}^{N} \left(\dot{b}_n(t) - \frac{\mathrm{i}}{\hbar} E_n b_n(t)\right) \exp\left(-\frac{\mathrm{i}}{\hbar} E_n t\right) |n\rangle = -\frac{\mathrm{i}}{\hbar} [H_0 + V(t)] \sum_{n=1}^{N} b_n(t) \exp\left(-\frac{\mathrm{i}}{\hbar} E_n t\right) |n\rangle \,, \tag{24}$$

which can be simplified to yield

$$\dot{b}_m(t) = \sum_{n=1}^{N} (i\hbar)^{-1} \langle m|V(t)|n\rangle b_n(t) \exp(i\omega_{mn}t) , \tag{25}$$

where

$$\omega_{mn} = \frac{1}{\hbar}(E_m - E_n) . \tag{26}$$

Next, if one replaces $V(t)$ by $\lambda V(t)$ and writes $b_n(t)$ as

$$b_n(t) = b_n^{(0)}(t) + \lambda b_n^{(1)}(t) + \lambda^2 b_n^{(2)}(t) + \lambda^3 b_n^{(3)}(t) + \dots , \tag{27}$$

one can equate powers of the perturbation parameter λ in eq. (25) to obtain

$$\dot{b}_m^{(l)}(t) = \sum_{n=1}^{N} (i\hbar)^{-1} \langle m|V(t)|n\rangle b_n^{(l-1)}(t) \exp(i\omega_{mn}t) \tag{28}$$

for $l = 1, 2, 3, \dots \infty$ while $\dot{b}_m^{(0)}(t) = 0$ and $b_m^{(0)}(t) =$ constant.

Then, assuming all $b_m^{(l)}(0) = 0$ for $l = 1, 2, 3, \dots \infty$, one finds:

$$\begin{aligned} b_m^{(l)}(t) &= \sum_{n=1}^{N} (i\hbar)^{-1} \int_0^t \langle m|V(t')|n\rangle b_n^{(l-1)}(t') \exp(i\omega_{mn}t')\, dt' \\ &= \sum_{n=1}^{N} \sum_{j=1}^{N_p} (i\hbar)^{-1} \langle m|V_j|n\rangle \\ &\quad \times \int_0^t \cos m(\alpha_j t' + \phi_j) b_n^{(l-1)}(t') \exp(i\omega_{mn}t')\, dt' , \end{aligned} \tag{29}$$

and using $b_m(0) = b_m^{(0)}(t) = c_m = \langle m|\psi(0)$, where $\psi(0) = \sum_{m=1}^{N} c_m |m\rangle$, one can iterate eq. (29) to obtain as many $b_m^{(l)}(t)$ terms as needed.

Finally, combining eqs. (3), (5), (23), and (27) and letting $\lambda = 1$, one can obtain an expression for Φ_{ST}. Then, since each $b_n^{(l)}(t)$ term in it contains a product of $l \langle m|V_j|n\rangle$ or $l B_1$ terms, Φ_{ST} can be considered as a power series in B_1 and can be written as follows:

$$\begin{aligned} \Phi_{ST} &= \sum_{l=0}^{l_{max}} \Phi_{ST}^{(l)} \\ &= \sum_{l=0}^{l_{max}} \sum_{p=0}^{l} \int_0^{\infty} \sum_{n,m=1}^{N} \langle n|Q_T|m\rangle b_n^{*(p)}(t) b_m^{(l-p)}(t) \exp(i\omega_{nm}t) f(t)\, dt , \end{aligned} \tag{30}$$

where l_{max} is the maximum order of perturbation theory to be considered.

4.1.2. Discussion

Note that initially in evaluating the $b_n^{(l)}(t)$ terms using eq. (29), one need only consider integrals of the form

$$\begin{aligned} \int_0^t e^{i\omega t'} dt' &= \frac{1}{i\omega}(e^{i\omega t} - 1), \quad \text{for } \omega \neq 0 , \\ &= t, \qquad\qquad \text{for } \omega = 0 . \end{aligned} \tag{31}$$

If $\omega \neq 0$ these integrals lead to more integrals of the same form as l increases. However, if $\omega = 0$, these integrals can lead to integrals including nonzero powers of t':

$$\int_0^t (t')^n e^{i\omega t'} dt' = e^{i\omega t} \sum_{r=0}^{n} (-1)^r \frac{n! t^{n-r}}{(n-r)!(i\omega)^{r+1}} - (-1)^n \frac{n!}{(i\omega)^{n+1}}, \quad \text{for } \omega \neq 0,$$

$$= \frac{t^{n+1}}{n+1}, \quad \text{for } \omega = 0. \tag{32}$$

These latter integrals, however, always lead to integrals of the same form for $n \geq 0$ and so should give no problems as one raises l.

Once all the $b_m^{(l)}(t)$ terms needed are found, one must use eq. (30) to find Φ_{ST}. Thus, one will need to evaluate integrals of the form

$$\int_0^\infty t^n e^{i\omega t} f(t)\, dt = (-i)^n \frac{\partial^n}{\partial \omega^n} \int_0^\infty e^{i\omega t} f(t)\, dt, \tag{33}$$

which gives, when $f(t)$ is an exponential decay

$$(-i)^n \frac{\partial^n}{\partial \omega^n} \mathscr{L}(\omega) = (-i)^n \frac{\partial^n}{\partial \omega^n} \frac{1}{\tau} \int_0^\infty e^{i\omega t} e^{-t/\tau} dt = (-i)^n \frac{\partial^n}{\partial \omega^n} \frac{1}{1 - i\omega\tau}$$

$$= (-i)^n \frac{\partial^n}{\partial \omega^n} \frac{1 + i\omega\tau}{1 + \omega^2\tau^2} = \frac{\tau^n n!}{(1 - i\omega\tau)^{n+1}} \tag{34}$$

and gives, when $f(t)$ is the Noyes time-dependence

$$(-i)^n \frac{\partial^n}{\partial \omega^n} \mathscr{N}(\omega) = (-i)^n \frac{\partial^n}{\partial \omega^n} \int_0^\infty e^{i\omega t} M t^{-3/2} e^{-A/t} dt$$

$$= (-i)^n \frac{\partial^n}{\partial \omega^n} \left(M \sqrt{\frac{\pi}{A}} \exp(-\sqrt{2A|\omega|}) \left[\cos(\sqrt{2A|\omega|}) + i \frac{\omega}{|\omega|} \sin(\sqrt{2A|\omega|}) \right] \right). \tag{35}$$

Comparing the functions $\mathscr{L}(\omega)$ and $\mathscr{N}(\omega)$ to the integrals yielding them (eqs. (34) and (35)), one can see several properties. Both integrals involve an oscillating term multiplied by a decaying term; that is, $(1/\tau)e^{-t/\tau}$ starts at $1/\tau$ and decays to zero while $Mt^{-3/2}e^{-A/t}$ begins at zero, quickly rises to a peak, and then at large times $t \gg A$ decays as $t^{-3/2}$. Each integral involves a characteristic time (τ or A), and as the frequency ω increases, more oscillations will occur in this characteristic time. Eventually there are so many oscillations that the integral has equal positive and negative parts, and these cancel out, forcing the integral to drop to zero. This explains the decay of each function to zero for large ω values. Also notice that each function has an imaginary part that rises from zero to a peak before decaying to zero. This peak is caused by the $i \sin \omega t$ term of $e^{i\omega t}$, and the maximum (or minimum for $\omega < 0$) value occurs when the first hump of $\sin \omega t$ overlaps best with $f(t)$, i.e. when ω is near $1/\tau$ or $1/A$. Finally, notice how both functions have symmetric real parts and antisymmetric imaginary parts. This is due simply to the symmetries of the real and imaginary parts of $e^{i\omega t}$.

Next, notice how the t^n terms in eqs. (34) and (35) lead to derivatives of the results obtained for $n = 0$, namely $\mathscr{L}(\omega)$ and $\mathscr{N}(\omega)$. Plots of these functions are shown in Fig. 1 via eq. (51). In general, both $\mathscr{L}(\omega)$ and $\mathscr{N}(\omega)$ give finite derivatives for all values of ω and $n \geq 0$. However, expansion of the exponent, sine, and cosine factors in $\mathscr{N}(\omega)$ to lowest order in $\sqrt{2A|\omega|}$ reveals a cusp:

$$\mathcal{N}(\omega) = M\sqrt{\frac{\pi}{A}}\exp(-\sqrt{2A|\omega|})\left(\cos(\sqrt{2A|\omega|}) + \mathrm{i}\frac{\omega}{|\omega|}\sin(\sqrt{2A|\omega|})\right)$$
$$\simeq M\sqrt{\frac{\pi}{A}}\left[1 + \left(\mathrm{i}\frac{\omega}{|\omega|} - 1\right)\sqrt{2A|\omega|}\right]. \tag{36}$$

Thus, at $\omega = 0$, there will be discontinuities in derivatives of $\mathcal{N}(\omega)$, and this may cause problems for higher orders of perturbation theory.

Nevertheless, since the Noyes time-dependence decays only as $t^{-3/2}$ for large t, $P_{ST}(t)$ oscillations at long times make significant contributions to Φ_{ST}. Thus, the Noyes time-dependence requires many more time steps in the numerical integration method than does the exponential time-dependence. This can be a strong incentive for using a perturbation theory method like that discussed here when one cannot use the rotating frame treatment.

4.2. Explicit evaluation to second order

4.2.1. Derivation

For $l_{max} = 2$, using eqs. (29) and (30) and the identities:

$$2\,\mathrm{Re}\,C = C + C^*, \tag{37}$$
$$\langle r|D|s\rangle = [\langle s|D|r\rangle]^*, \tag{38}$$

where C is a complex number and D is a Hermitian operator such as Q_T or V_j, one obtains the following equations:

$$\Phi_{ST} = \Phi_{ST}^{(0)} + \Phi_{ST}^{(1)} + \Phi_{ST}^{(2)}, \tag{39}$$
$$\Phi_{ST}^{(0)} = \int_0^\infty \sum_{r,s=1}^{N} \langle r|Q_T|s\rangle b_r^{*(0)}(t) b_s^{(0)}(t) \exp(\mathrm{i}\omega_{rs}t) f(t)\,\mathrm{d}t \tag{40}$$
$$= \sum_{r,s=1}^{N} \langle r|Q_T|s\rangle c_r^* c_s \int_0^\infty \exp(\mathrm{i}\omega_{rs}t) f(t)\,\mathrm{d}t, \tag{41}$$
$$\Phi_{ST}^{(1)} = \int_0^\infty \sum_{r,s=1}^{N} \langle r|Q_T|s\rangle\,[c_r^* b_s^{(1)}(t) + b_r^{*(1)}(t) c_s] \exp(\mathrm{i}\omega_{rs}t) f(t)\,\mathrm{d}t \tag{42}$$
$$= \int_0^\infty \sum_{r,s=1}^{N} 2\,\mathrm{Re}[\langle r|Q_T|s\rangle c_r^* b_s^{(1)}(t) \exp(\mathrm{i}\omega_{rs}t)] f(t)\,\mathrm{d}t \tag{43}$$
$$= \sum_{r,s,n=1}^{N} \sum_{j=1}^{N_p} 2\,\mathrm{Re}\left(\langle r|Q_T|s\rangle \frac{c_r^* c_n}{\mathrm{i}\hbar} \langle s|V_j|n\rangle \int_0^\infty \exp(\mathrm{i}\omega_{rs}t) f(t)\,\mathrm{d}t \int_0^t \cos(\alpha_j t' + \phi_j) \exp(\mathrm{i}\omega_{sn}t')\,\mathrm{d}t'\right), \tag{44}$$

$$\Phi_{ST}^{(2)} = \int_0^\infty \sum_{r,s=1}^{N} \langle r|Q_T|s\rangle \left[c_r^* b_s^{(2)}(t) + b_r^{*(1)}(t) b_s^{(1)}(t) + b_r^{*(2)}(t) c_s\right] \exp(i\omega_{rs}t) f(t)\, dt \tag{45}$$

$$= \int_0^\infty \sum_{r,s=1}^{N} \left\{\langle r|Q_T|s\rangle b_r^{*(1)}(t) b_s^{(1)}(t) \exp(i\omega_{rs}t) + 2\,\mathrm{Re}\left[\langle r|Q_T|s\rangle c_r^* b_s^{(2)}(t) \exp(i\omega_{rs}t)\right]\right\} f(t)\, dt \tag{46}$$

$$= \sum_{r,s,m,n=1}^{N} \sum_{j,k=1}^{N_p} \langle r|Q_T|s\rangle \frac{c_n^* c_m}{(i\hbar)^2} \langle n|V_j|r\rangle\langle s|V_k|m\rangle$$

$$\times \int_0^\infty \exp(i\omega_{rs}t) f(t)\, dt \left(\int_0^t \cos(\alpha_j t' + \phi_j) \exp(i\omega_{nr}t')\, dt'\right)\left(\int_0^t \cos(\alpha_k t' + \phi_k) \exp(i\omega_{sm}t')\, dt'\right)$$

$$+ \sum_{r,s,m,n=1}^{N} \sum_{j,k=1}^{N_p} 2\,\mathrm{Re}\left[\langle r|Q_T|s\rangle \frac{c_r^* c_m}{(i\hbar)^2} \langle s|V_j|n\rangle\langle n|V_k|m\rangle\right.$$

$$\left.\times \int_0^\infty \exp(i\omega_{rs}t) f(t)\, dt \left(\int_0^t \cos(\alpha_j t' + \phi_j) \exp(i\omega_{sn}t')\, dt' \int_0^{t'} \cos(\alpha_k t'' + \phi_k) \exp(i\omega_{nm}t'')\, dt''\right)\right]. \tag{47}$$

Then, integrating all the above terms and pooling some more complex conjugates gives

$$\Phi_{ST}^{(0)} = \sum_{r,s=1}^{N} \langle r|Q_T|s\rangle c_r^* c_s \mathscr{A}(\omega_{rs}),$$

$$\Phi_{ST}^{(1)} = \sum_{r,s,n=1}^{N} \sum_{j=1}^{N_p} \mathrm{Re}\left(\langle r|Q_T|s\rangle \frac{c_r^* c_n}{-\hbar} \langle s|V_j|n\rangle \left[\exp(i\phi_j)\mathscr{B}(\omega_{rs}, \omega_{sn} + \alpha_j) + \exp(-i\phi_j)\mathscr{B}(\omega_{rs}, \omega_{sn} - \alpha_j)\right]\right),$$

$$\Phi_{ST}^{(2)} = \sum_{r,s,m,n=1}^{N} \sum_{j,k=1}^{N_p} \mathrm{Re}\left[\langle r|Q_T|s\rangle \frac{c_n^* c_m}{-2\hbar^2} \langle n|V_j|r\rangle\langle s|V_k|m\rangle \exp(i\phi_j) \exp(i\phi_k)\mathscr{C}(\omega_{rs}, \omega_{nr} + \alpha_j, \omega_{sm} + \alpha_k)\right]$$

$$+ \sum_{r,s,m,n=1}^{N} \sum_{j,k=1}^{N_p} \langle r|Q_T|s\rangle \frac{c_n^* c_m}{-4\hbar^2} \langle n|V_j|r\rangle\langle s|V_k|m\rangle \left[\exp(-i\phi_j) \exp(i\phi_k)\mathscr{C}(\omega_{rs}, \omega_{nr} - \alpha_j, \omega_{sm} + \alpha_k)\right.$$

$$\left.+ \exp(i\phi_j) \exp(-i\phi_k)\mathscr{C}(\omega_{rs}, \omega_{nr} + \alpha_j, \omega_{sm} - \alpha_k)\right]$$

$$+ \sum_{r,s,m,n=1}^{N} \sum_{j,k=1}^{N_p} \mathrm{Re}\left(\langle r|Q_T|s\rangle \frac{c_r^* c_m}{2\hbar^2} \langle s|V_j|n\rangle\langle n|V_k|m\rangle \left[\exp(i\phi_j) \exp(i\phi_k)\mathscr{D}(\omega_{rs}, \omega_{sn} + \alpha_j, \omega_{nm} + \alpha_k)\right.\right.$$

$$+ \exp(-i\phi_j) \exp(i\phi_k)\mathscr{D}(\omega_{rs}, \omega_{sn} - \alpha_j, \omega_{nm} + \alpha_k)$$

$$+ \exp(i\phi_j) \exp(-i\phi_k)\mathscr{D}(\omega_{rs}, \omega_{sn} + \alpha_j, \omega_{nm} - \alpha_k)$$

$$\left.\left.+ \exp(-i\phi_j) \exp(-i\phi_k)\mathscr{D}(\omega_{rs}, \omega_{sn} - \alpha_j, \omega_{nm} - \alpha_k)\right]\right), \tag{48}$$

where the four lineshape functions $\mathscr{A}$–$\mathscr{D}$ are defined for the exponential case as follows:

$$\mathscr{A}(\omega)=\mathscr{L}(\omega), \qquad \mathscr{B}(\omega,\Delta)=\frac{1}{\Delta}[\mathscr{L}(\omega+\Delta)-\mathscr{L}(\omega)],$$

$$\mathscr{C}(\omega,\Delta,\delta)=\frac{1}{\Delta\delta}[\mathscr{L}(\omega+\Delta+\delta)-\mathscr{L}(\omega+\Delta)-\mathscr{L}(\omega+\delta)+\mathscr{L}(\omega)],$$

$$\mathscr{D}(\omega,\Delta,\delta)=\frac{1}{\delta}\left(\frac{\mathscr{L}(\omega+\Delta+\delta)-\mathscr{L}(\omega)}{\Delta+\delta}-\frac{\mathscr{L}(\omega+\Delta)-\mathscr{L}(\omega)}{\Delta}\right), \tag{49}$$

where ω is always an eigenfrequency of H_0 (such as ω_{rs}) and Δ and δ are always sums of an eigenfrequency of H_0 with one of the frequencies of the time-dependent field ($\Delta=\omega_{rs}+\alpha_j$, for example). Note that for the case of the Noyes time-dependence, all $\mathscr{L}$'s can simply be replaced by $\mathscr{N}$'s.

Also note that since $\mathscr{L}^*(\omega)=\mathscr{L}(-\omega)$, the following hold true:

$$\mathscr{A}^*(\omega)=\mathscr{A}(-\omega), \quad \mathscr{B}^*(\omega,\Delta)=-\mathscr{B}(-\omega,-\Delta), \quad \mathscr{C}^*(\omega,\Delta,\delta)=\mathscr{C}(-\omega,-\Delta,-\delta),$$
$$\mathscr{D}^*(\omega,\Delta,\delta)=\mathscr{D}(-\omega,-\Delta,-\delta). \tag{50}$$

These relations are useful in the discussion below.

4.2.2. Discussion

The terms in eq. (48) have a number of interesting properties:

(i) Each term is either real or has its complex conjugate listed. This is as expected since the singlet-to-triplet yield should always be real. It is not difficult to show that the three terms not explicitly listed as real in eq. (48) have their complex conjugates listed. Swapping r for s gives the $\Phi_{ST}^{(0)}$ term's complex conjugate and swapping r for s, m for n, and j for k gives the two $\Phi_{ST}^{(2)}$ terms' complex conjugates. Note that if the $\Phi_{ST}^{(0)}$ term has $r=s$, it is already a real number. The same holds for the $\Phi_{ST}^{(2)}$ terms when $r=s$, $m=n$, and $j=k$, since each term is then a real number times $\mathscr{C}(0,\Delta,-\Delta)$, which is also a real number.

(ii) The perturbations V_j begin to interact with each other at second order. Thus, even though at first order (weak oscillating fields) the overall effect of multiple perturbations is just the sum of the effects of the individual perturbations, at higher orders (strong oscillating fields) the overall effect is a nonlinear combination of the effects of the individual perturbations. Examples of such nonlinear effects are given in Fig. 6.

(iii) Each term is like a circular chain of matrix elements (links) connecting different eigenstates of H_0. Each eigenstate involved in the chain appears an even number of times in the row and column numbers of the matrix elements in the chain. Each chain also always includes one $\langle r|Q_T|s\rangle$ link, one $c_r^* c_m$ link, and l $\langle s|V_j|n\rangle$ perturbation links, and each perturbation link $\langle s|V_j|n\rangle$ always comes with a leading factor $(1/2\hbar)e^{\pm i\phi_j}$ and a lineshape function like $\mathscr{B}$, $\mathscr{C}$, or $\mathscr{D}$ that includes a denominator like $(\omega_{sn}\pm\alpha_j)$ or $(\omega_{sn}\pm\alpha_j+\omega_{nm}\pm\alpha_k)$.

The lineshape functions in eq. (49) also have a number of interesting properties:

(i) Since they all depend on $\mathscr{L}$ (or $\mathscr{N}$), the terms $\mathscr{A}$–$\mathscr{D}$ all decay to zero as ω, Δ, or δ grows very large.

(ii) The higher order terms $\mathscr{B}$–$\mathscr{D}$ are largest when Δ or δ approaches zero, that is, as the perturbation frequencies α_j and α_k approach eigenfrequencies of the steady Hamiltonian H_0. Using l'Hôpital's rule, one can obtain these terms in the $\Delta=\delta=0$ limit:

$$\mathscr{A}(\omega)=\mathscr{L}(\omega), \qquad \mathscr{B}(\omega,0)=\frac{\partial\mathscr{L}(\omega)}{\partial\omega}, \qquad \mathscr{C}(\omega,0,0)=\frac{\partial^2\mathscr{L}(\omega)}{\partial\omega^2},$$

$$\mathscr{D}(\omega,0,0)=\frac{1}{2}\frac{\partial^2\mathscr{L}(\omega)}{\partial\omega^2}=\tfrac{1}{2}\mathscr{C}(\omega,0,0). \tag{51}$$

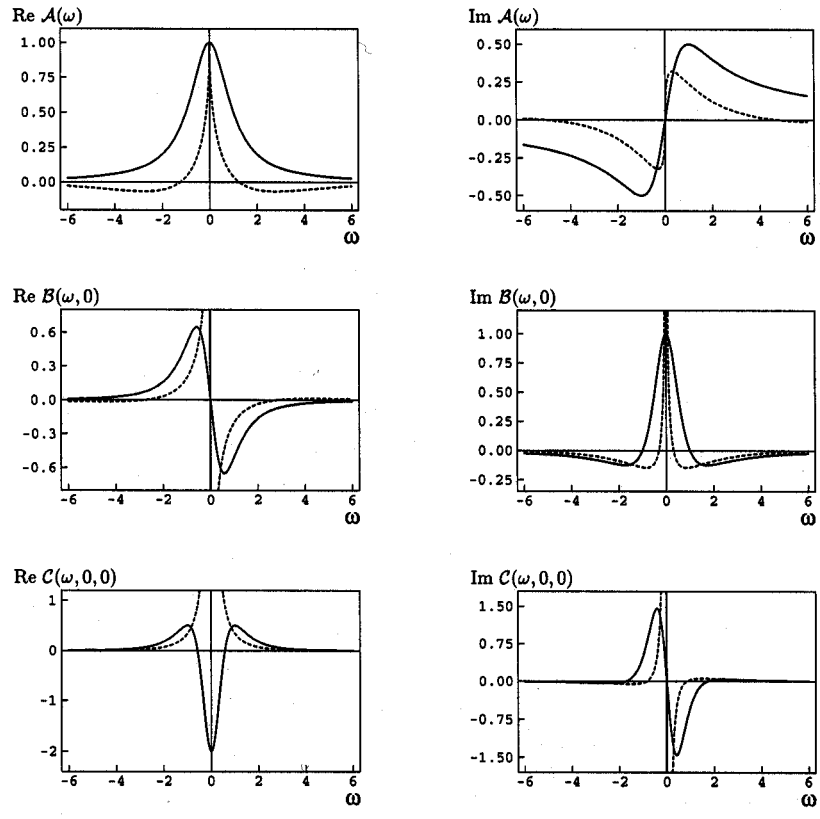

Fig. 1. Real and imaginary parts of functions $\mathscr{A}$–$\mathscr{C}$ as given in eq. (51) for exponential (solid lines) and Noyes (dotted lines) time-dependences when $\tau = A = 1$ and $M = \sqrt{A/\pi}$.

Plots of these for both the exponential and Noyes time-dependences are shown in Fig. 1. Notice that in this limit, as shown in eq. (34), $\partial^n \mathscr{L}(\omega)/\partial\omega^n$ scales as τ^n. Thus, in this limit the perturbation series becomes an expansion in powers of τ.

(iii) Since $\mathscr{L}(\omega)$ and its derivatives are largest for small ω, the smallest eigenfrequencies of H_0 should dominate the dynamics. Of course, since the bandwidth of $\mathscr{L}(\omega)$ is determined by $1/\tau$, for small τ this effect is not so apparent. However, as τ increases, one expects fewer and fewer eigenfrequencies to matter until eventually only pairs of degenerate energy levels matter. In this extreme $\omega = 0$ limit, the four different terms become:

$$\mathscr{A}(0) = 1, \qquad \mathscr{B}(0, \Delta) = \frac{1}{\Delta}[\mathscr{L}(\Delta) - 1], \qquad \mathscr{C}(0, \Delta, \delta) = \frac{1}{\Delta\delta}[\mathscr{L}(\Delta+\delta) - \mathscr{L}(\Delta) - \mathscr{L}(\delta) + 1],$$

$$\mathscr{D}(0, \Delta, \delta) = \frac{1}{\delta}\left(\frac{\mathscr{L}(\Delta+\delta) - 1}{\Delta+\delta} - \frac{\mathscr{L}(\Delta) - 1}{\Delta}\right). \tag{52}$$

Plots of these are shown in Fig. 2 for the exponential case and for the Noyes time-dependence.

(iv) The functions $\mathscr{C}$ and $\mathscr{D}$ are related. Using eq. (49) one can easily obtain the following:

$$\mathscr{C}(\omega, \Delta, \delta) = \mathscr{C}(\omega, \delta, \Delta) = \mathscr{D}(\omega, \Delta, \delta) + \mathscr{D}(\omega, \delta, \Delta), \tag{53}$$

$$\mathscr{C}(\omega, \Delta, \Delta) = 2\mathscr{D}(\omega, \Delta, \Delta) = \frac{1}{\Delta^2}[\mathscr{L}(\omega+2\Delta) - 2\mathscr{L}(\omega+\Delta) + \mathscr{L}(\omega)]. \tag{54}$$

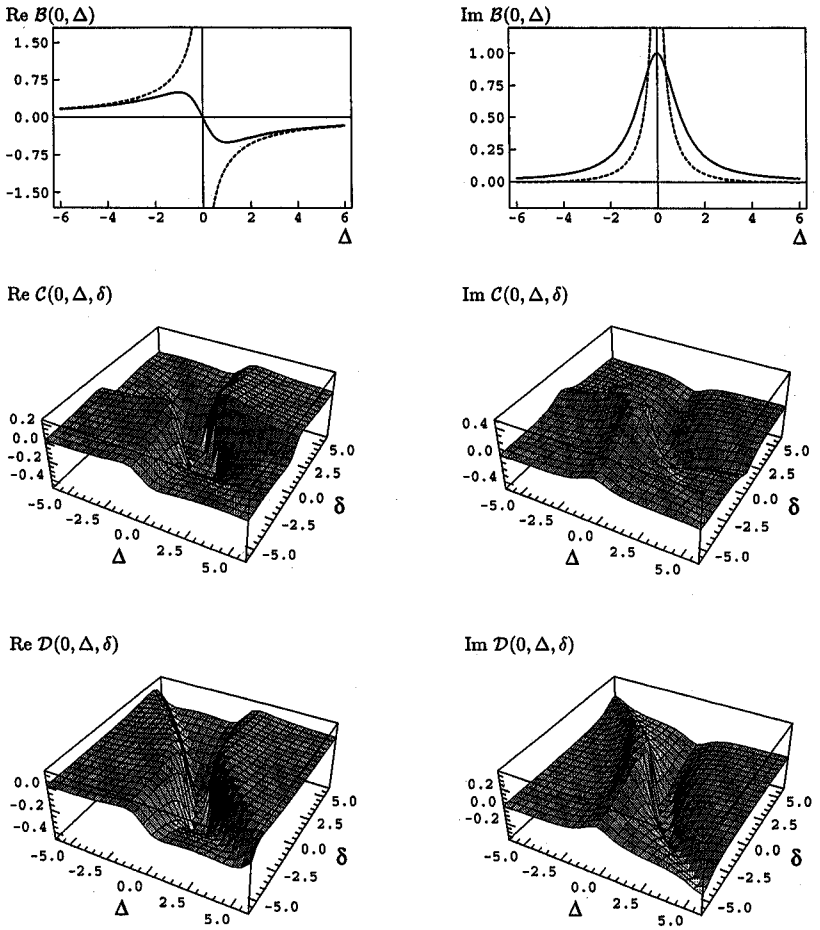

Fig. 2. Real and imaginary parts of functions $\mathcal{B}$–$\mathcal{D}$ as given in eq. (52) for the exponential time-dependence (shown in all plots) and for the Noyes time-dependence (dotted lines in plots of $\mathcal{B}$) when $\tau = A = 1$ and $M = \sqrt{A/\pi}$. Plots of functions $\mathcal{E}$–$\mathcal{D}$ for the Noyes time-dependence (not shown) resemble the ones given here for the exponential case but have much sharper features. Note that the plots of $\mathcal{E}(0, \Delta, \delta)$ and $\mathcal{D}(0, \Delta, \delta)$ have been truncated and so do not show absolute extrema. Nontruncated cross sections of these plots are given in Fig. 3.

One can easily verify these results for $\omega = 0$ by visual inspection of Fig. 2. Eq. (54) is plotted in Fig. 3 for $\omega = 0$ for both the exponential and Noyes time-dependences.

(v) Using eq. (53) it may be possible to simplify the $\Phi_{ST}^{(2)}$ terms in eq. (48) that include $\mathcal{D}(\omega, \Delta, \delta)$. By

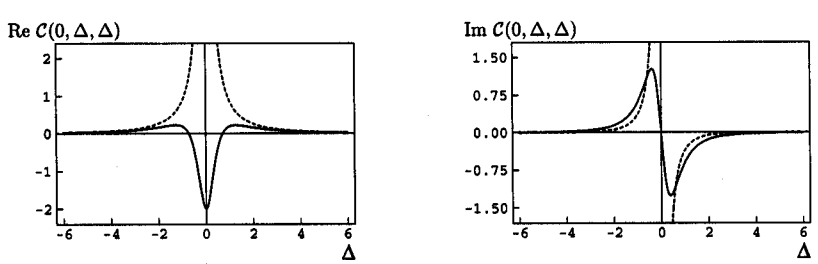

Fig. 3. Real and Imaginary parts of function $\mathcal{E}(0, \Delta, \Delta)$ as given in eq. (54) for exponential (solid lines) and Noyes (dotted lines) time-dependences when $\tau = A = 1$ and $M = \sqrt{A/\pi}$. These plots show the extrema that were truncated in Fig. 2.

symmetry it seems that this should be possible; that is, overall one would expect the perturbations $V_j \cos(\alpha_j t + \phi_j)$ and $V_k \cos(\alpha_k t + \phi_k)$ to be interchangeable. This interchangeability is apparent in the $\mathscr{E}(\omega, \Delta, \delta)$ terms in which Δ and δ have equivalent roles; however, it seems prohibited by the $\mathscr{D}(\omega, \Delta, \delta)$ terms which treat Δ and δ quite differently (as shown in eqs. (49) and (52) and in Fig. 2).

(vi) Finally, there is a symmetry difference (consistently shown in Figs. 1–3) between the real and imaginary parts of each term; that is, each term typically has one symmetric part and one antisymmetric part. Thus, the symmetry of a term's overall contribution to the singlet-to-triplet yield waveform is determined by the overall real and imaginary contributions of all the links in the chain for the term.

5. Sample results

5.1. Comparison of methods

Sample calculations done for the exponential case with the three methods described are given in Figs. 4 and 5. Fig. 4 reproduces results given in Fig. 1 of Ref. [12] for a typical RYDMR lineshape. Fig. 5 uses almost the same parameters as Fig. 4 but instead shows effects of rotating and linear oscillating fields for a system in a 0.5 G steady

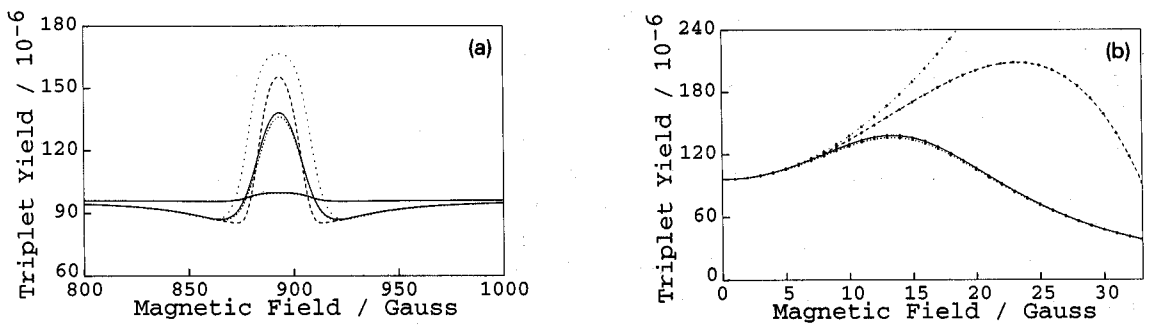

Fig. 4. Comparison of singlet-to-triplet yields calculated using Runge–Kutta (finely dotted lines), rotating frame (solid lines), and perturbation ($l_{max}=2$ is sparsely dotted, $l_{max}=4$ is dashed) methods. Here $g=2$, $\boldsymbol{B}_1(t)$ is a rotating field applied perpendicular to $\boldsymbol{B}_0$ at frequency 2.5 GHz, only one nuclear spin with $I_1=\frac{1}{2}$ and $a_1=0.5$ G is included, $J=14$ G (39.18913 MHz), and $\tau=5$ ns. Runge–Kutta points use $N_t=5000$ and $\delta t=0.03$ ns. (a) B_0 varies from 800 to 1000 G for $B_1=3$ G (lower curves) and 13 G (upper curves). (b) B_0 is fixed at resonance (893.1053 G) and B_1 is varied from 0 to 33 G.

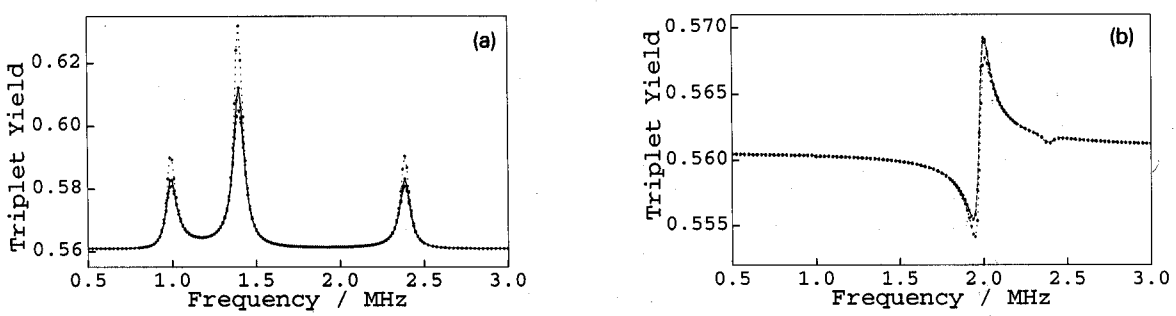

Fig. 5. Comparison of singlet-to-triplet yields calculated using Runge–Kutta (finely dotted lines), rotating frame (solid lines), and perturbation methods. Here $g=2$, $B_0=0.5$ G, $\boldsymbol{B}_1(t)$ oscillates at frequencies from 0.5 to 3 MHz and has $B_1=0.007$ G, only one nuclear spin with $I_1=\frac{1}{2}$ and $a_1=0.5$ G is included, $J=0$, and $\tau=5000$ ns. The larger τ used here is needed to resolve the smaller frequencies shown. Runge–Kutta points use $N_t=10000$ and $\delta t=15$ ns. (a) $\boldsymbol{B}_1(t)$ rotates about $\boldsymbol{B}_0$. $l_{max}=2$ is sparsely dotted, $l_{max}=4$ is dashed. (b) $\boldsymbol{B}_1(t)$ is a linear oscillation along $\boldsymbol{B}_0$. $l_{max}=1$ is sparsely dotted, $l_{max}=2$ is dashed. Results from rotating frame (inapplicable here) are not shown.

field. Figs. 4 and 5 show good agreement among the three different methods and show how the results from perturbation theory vary with the maximum order of perturbation theory used (l_{max}). Finally, Fig. 4 shows the breakdown of perturbation theory as the oscillating field strength B_1 rises.

Note that in Figs. 4 and 5 the Runge–Kutta and rotating frame methods always agree best, often giving indistinguishable curves in the plots. The perturbation method, however, is indistinguishable from the other methods only when B_1 is small, as shown in the $B_1 = 3$ G curves of Fig. 4a and the $B_1 < 6$ G region of Fig. 4b. Also note that as l_{max} rises, the perturbation method's results tend to approach those of the other two methods. In fact, in Fig. 5b, while the results from the perturbation method at $l_{max} = 1$ stand apart, the results at $l_{max} = 2$ are virtually indistinguishable from the Runge–Kutta results.

Interestingly, in Fig. 4b the three methods agree quite well out to $B_1 = 10$ G. This is somewhat surprising since the smallest term in H_0 is a hyperfine interaction with $a_1 = 0.5$ G. Thus, one would expect the perturbation method to fail for much smaller B_1 values. Instead it seems that the next largest term in H_0, the exchange interaction with $J = 14$ G, is acting as the cutoff. Also note that Fig. 4 shows slight differences between the Runge–Kutta and rotating frame methods when B_1 is about 13 G and the system is near resonance. These differences drop from roughly 2% (shown) to under 0.02% when N_t and δt are changed to 15000 and 0.01 ns respectively. Apparently at resonance $B_1 = 13$ G gives faster oscillations in $P_{ST}(t)$ than the other points and thus requires smaller Runge–Kutta time steps to evaluate Φ_{ST}.

Finally, note that in Figs. 4 and 5a, for rotating fields, only even values of l_{max} are shown. This is because results for $l_{max} = 0$ and 1 are the same, results for $l_{max} = 2$ and 3 are the same, and results for $l_{max} = 4$ and 5 are the same. That is, only even orders of perturbation theory are contributing to the singlet-to-triplet yields. This can be further verified by noting that in Fig. 4b the $l_{max} = 2$ results scale as B_1^2 while the difference between the $l_{max} = 4$ and $l_{max} = 2$ results scales as B_1^4.

This phenomenon is due to the symmetry of the restricted class of systems examined here. In each system, since all the spin Hamiltonian parameters used are isotropic, only the magnetic field gives some asymmetry; that is, the steady field sets up an oriented axis. When the time-dependent field rotates about this axis, only its magnitude, not its direction in the plane perpendicular to this axis, matters. Thus, only terms including even powers of B_1 will be allowed in the perturbation expansion. Thus, only even orders of perturbation theory matter. Similar arguments hold for linear fields oscillating perpendicular to the steady field.

Nevertheless, if the time-dependent field is a linear oscillation along $\boldsymbol{B}_0$ (as in Fig. 5b), the sign of B_1 matters, and this allows odd orders of perturbation theory to matter as well. In fact, any asymmetry in the spin Hamiltonian parameters or magnetic field configuration that can make the sign (direction) of a particular oscillating field matter can allow odd orders of perturbation theory to matter. Such asymmetries can speed up calculations since one can stop after first order for small enough B_1 values.

5.2. Execution times

Typical CPU times needed to calculate each point in Figs. 4 and 5 using IBM RS6000/320H and IRIS Crimson/R4000 workstations are shown in Table 1. One can easily make a coarse estimate of how these times depend on N, N_S, N_p, and N_t, especially for large values when only the highest power terms matter. First, since $N_S = \frac{1}{4}N$ when the initial state is singlet and $N_S = \frac{3}{4}N$ when it is triplet, if one neglects leading factors, one can replace N_S by N. Then, since both the perturbation and rotating frame methods require diagonalization of H_0 to obtain eigenvalues and eigenvectors, the time they require to execute on a computer scales at the minimum as N^3 [21]. Also, since both of these methods require several matrix multiplications to evaluate the $\langle r|Q_T|s\rangle$ and c_m elements used, more terms scaling as N^3 must be added to the total. Meanwhile, evaluating $\langle s|V_j|n\rangle$ scales as $N^3 N_p$, but these matrix elements are only needed for $l_{max} > 0$, and other terms are more dominant then. Thus, since the rotating frame and perturbation methods at $l_{max} = 0$ are equivalent, counting up terms in eq. (48) or in eqs. (29) and (30) and averaging over the N_S different initial states, one sees that while the rotating frame method always scales as N^3, the perturbation method scales roughly as $N^{3+l_{max}} N_p^{l_{max}}$, soon becoming much slower than the rotating frame method. Meanwhile, the Runge–

Table 1
Typical times spent on two common workstations calculating each point in figs. 4 and 5 where $N=8$ and $N_p=1$

Figure	Method	Time (CPU seconds)		Estimated scaling/N^3
		IBM RS6000/320H	IRIS Crimson/R4000	
4	Runge–Kutta ($N_t=5000$)	129.86	25.90	5000
5a	Runge–Kutta ($N_t=10000$)	263.15	51.82	10000
5b	Runge–Kutta ($N_t=10000$)	260.33	51.70	10000
4	rotating frame	0.07	0.02	1
5a	rotating frame	0.07	0.05	1
5b	perturbation ($l_{max}=1$)	1.38	0.29	8
4	perturbation ($l_{max}=2$)	4.73	0.70	64
5a	perturbation ($l_{max}=2$)	4.33	0.54	64
5b	perturbation ($l_{max}=2$)	2.79	0.48	64
4	perturbation ($l_{max}=4$)	473.03	33.02	4096
5a	perturbation ($l_{max}=4$)	386.20	11.72	4096

Kutta method's execution time is dominated by a number of matrix multiplications done at each time step (all scaling as N^3), and so it scales as N^3N_t (N_t = number of time steps, typically 1000 or more). Thus, for small l_{max} and N values (N is always $\geqslant 4$, and if any hyperfine interaction is included is $\geqslant 8$), the perturbation theory method can go much faster than the Runge–Kutta method, but as l_{max} increases, the perturbation theory method soon becomes much slower than the Runge–Kutta method.

The systems shown in Figs. 4 and 5 all have $N=8$ and $N_p=1$, numbers that should let the perturbation method go very fast. Estimates of scaling factors using expressions from the previous paragraph and these N and N_p values are given in Table 1. Note that the perturbation method's execution time does not always rise as quickly with l_{max} as estimated above and that this method's execution time depends not just on the size N of the Hamiltonian used but also on its specific contents (see $l_{max}=4$ results, for example). These effects are probably due to the pooling of terms with equal $t^n e^{i\omega t}$ factors when evaluating eqs. (29) and (30) in the computer program used. Also notice how the times on the two workstations used are not simply proportional to each other. Thus, it may not be so simple to obtain more accurate estimates.

To further explore these scaling relations it is useful to vary N. Table 2 shows how typical execution times change with N using the parameters of Fig. 4 and letting $I_1=\frac{1}{2}$, $\frac{3}{2}$, or $\frac{7}{2}$. From these times one can estimate the effective scaling. Surprisingly, Table 2 shows that the program performs better than estimated above on all calculations. Since neither workstation is a vector processor, this may be due to the large number of zeroes in the Hamiltonian matrices for the systems used or to the isotropy of these systems giving many degenerate eigenvalues. One would expect the former factor to speed matrix multiplications and the latter factor to reduce the total number of different $t^n e^{i\omega t}$ terms in the perturbation method. Both factors might also speed diagonalizations. Nevertheless, using the

Table 2
Typical times spent on two common workstations calculating points as if in fig. 4 but with $I_1=\frac{1}{2}$, $\frac{3}{2}$, and $\frac{7}{2}$ ($N=8$, 16, and 32) and $N_p=1$

Method	Time (CPU seconds)						Effective scaling	Estimated scaling
	IBM RS6000/320H			IRIS Crimson/R4000				
	$N=8$	$N=16$	$N=32$	$N=8$	$N=16$	$N=32$		
Runge–Kutta ($N_t=5000$)	129.86	337.41	1296.45	25.90	79.43	384.64	$N^{1-3}N_t$	N^3N_t
rotating frame	0.07	0.18	0.77	0.02	0.07	0.31	N^{1-3}	N^3
perturbation ($l_{max}=2$)	4.73	35.11	214.29	0.70	4.51	27.82	N^{2-3}	N^5
perturbation ($l_{max}=4$)	473.03	9051.68	37016.69	33.02	445.75	1492.07	N^{1-5}	N^7

effective scaling relations given in Table 2 and the calculation times given in both tables, one can extrapolate execution times to other values of N.

5.3. Other results

In addition to comparing the different calculation methods, Figs. 4 and 5 show phenomena that may be important to magnetic field bioeffects researchers:

(i) Fig. 4 shows the nonlinearity inherent in the radical pair mechanism; that is, the effects on the singlet-to-triplet yields do not always increase as one raises the oscillating field strength. Thus, if this mechanism does indeed account for some of the magnetic field effects in biology, one should not expect simple dose–response curves.

(ii) Fig. 5 shows the need for careful control of field orientations; that is, simply by changing the orientation of the oscillating field, one can dramatically alter the singlet-to-triplet yield versus frequency spectrum. The lineshapes can change symmetry, and the optimal frequencies (frequencies of maximum/minimum yield) can shift. Such spectral changes due to poor control of oscillating field orientation may account for some of the conflicts in the literature on biological magnetic field effects.

Another phenomenon that may be important to magnetic field bioeffects researchers is shown in Fig. 6. It shows that the effects of two simultaneously applied oscillating fields do not simply sum together; instead, they interact in a nonlinear fashion (in particular note the interaction of 1.4 MHz with 1 MHz or 2.4 MHz fields). Such nonlinear interactions (due to second order and higher perturbation expansion terms) of experimentally applied fields, which become more apparent at higher oscillating field strenghts, with uncontrolled environmental fields may account for some of the conflicts in the literature on biological magnetic field effects. Thus, careful shielding of stray oscillating fields and the application of very weak experimental oscillating fields are recommended.

Note that the singlet-to-triplet yields in Fig. 4 are much smaller than those in Figs. 5 and 6. Nevertheless, those in Fig. 4 show much larger relative variations in yield due to oscillating fields than do those in Figs. 5 and 6. The small yields in Fig. 4 are due to the exchange interaction which energetically separates the singlet state from the triplet states. For most oscillating field frequencies, transitions between these separated states are not favored, and so there is little mixing between the singlet and triplet states, and so there are very small yields. Nevertheless, certain oscillating fields connect the states, allow mixing, and so dramatically affect the yields. In Figs. 5 and 6, however, the singlet and triplet states are already very close in energy, and this gives a large baseline mixing. Thus, their yields tend to be higher, and so the relative changes induced by the oscillating fields tend to be smaller.

Finally, Figs. 7 and 8 compare results for the exponential and Noyes time-dependences for the systems shown in Figs. 4 and 5. Typically the Noyes time-dependence just gives sharper peaks. Nevertheless, notice the stark contrast between the results for the two time-dependences shown in Fig. 7. Such differences point out the usefulness of RYDMR for differentiating the types of diffusive motion possible in radical intermediates.

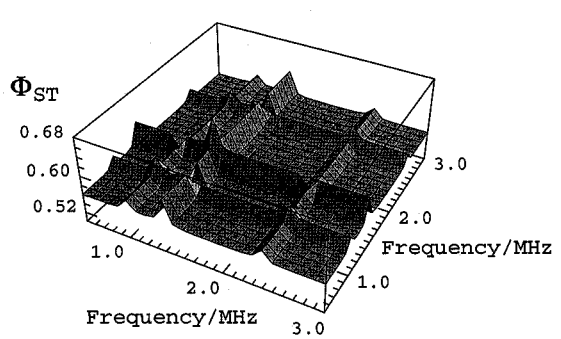

Fig. 6. Singlet-to-triplet yields calculated using Runge–Kutta method when two perturbations (each with $B_1 = 0.007$ G) act simultaneously. Here $\boldsymbol{B}_1(t)$ is composed of two fields rotating about $\boldsymbol{B}_0$ at independent frequencies. All other parameters as in fig. 5.

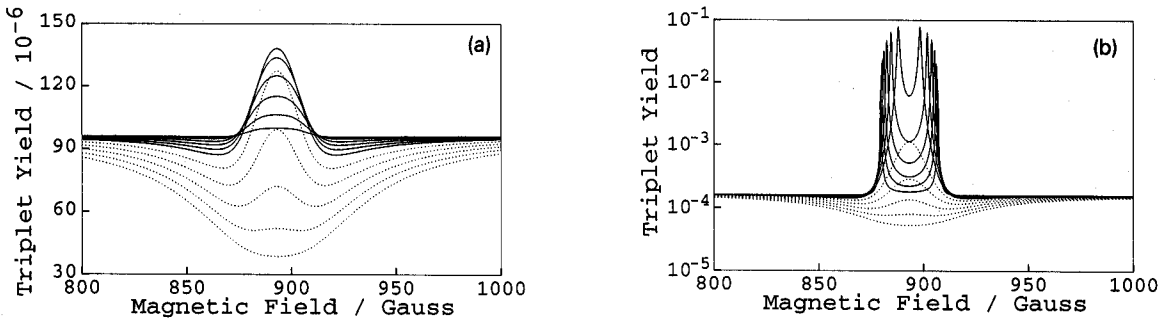

Fig. 7. Singlet-to-triplet yields calculated using rotating frame method for (a) exponential and (b) Noyes time-dependences. Parameters as in fig. 4a but $A = 5$ ns and $M = \sqrt{A/\pi}$ in (b). Solid curves rise as B_1 rises from 3 to 13 G in 2 G steps. Dotted curves drop as B_1 rises from 17 to 33 G in 4 G steps. The curves in (a) are plotted linearly to match those shown and discussed in depth in fig. 1 of ref. [12]. The curves in (b) are plotted logarithmically to show more detail.

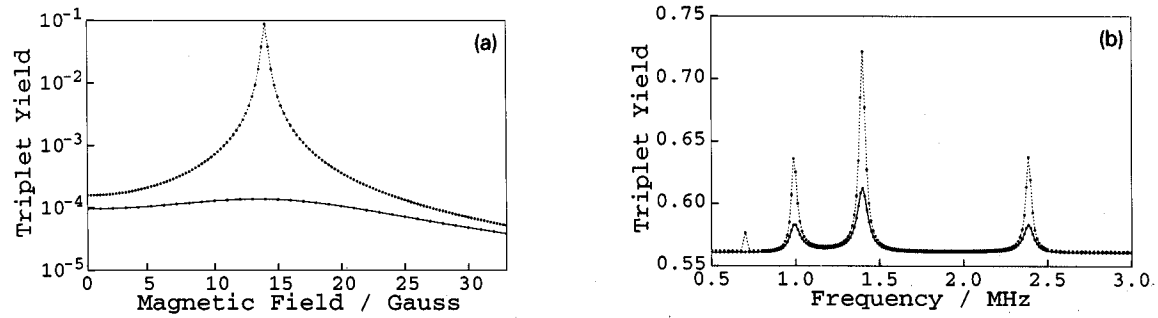

Fig. 8. Singlet-to-triplet yields calculated using rotating frame method for exponential (solid lines) and Noyes (dotted lines) time-dependences. Parameters as in figs. 4b and 5a but $A = 5$ or 5000 ns and $M = \sqrt{A/\pi}$ for the Noyes time-dependence curves.

Also notice that the singlet-to-triplet yield curves for the Noyes time-dependence are all finite despite the divergent terms that must be contributing to them, even at the lowest orders of perturbation theory. This is reminiscent of problems approached by use of the renormalization group [24].

6. Conclusion

The perturbation theory method developed in this paper is useful because it gives insight into the shape of the frequency dependence and leads to analytical expressions which show what matrix elements most affect the singlet-to-triplet yields. It can handle multiple oscillating fields with no restrictions on their orientations or frequencies. It also applies for anisotropic Zeeman, hyperfine, or exchange interactions or when other more complicated interactions are included. It inherently works best when only the lowest orders of perturbation theory are needed, that is, when the oscillating fields are very weak with respect to the steady field, which happens in nature as well as in man-made environments.

It is hoped that this derivation will inspire more work. Surely somewhere in its equations lies a fast heuristic method that can tell which frequencies and field orientations will most affect a particular system. Such a method would be useful for scouting out a wide variety of field configurations for many different spin systems looking for interesting or optimal effects. One could then explore more rigorously the specific systems found using a slower method such as the Runge–Kutta method. Such a fast heuristic method would be useful for finding candidate reactions that could explain some of the magnetic field effects seen in biology.